Analysis of particles size distributions in Mg(OH)2 precipitation from highly concentrated MgCl2 solutions

Powder Technology 398 (2022) 117106

Contents lists available at ScienceDirect

Powder Technology

journal homepage: www.elsevier.com/locate/powtec

Analysis of particles size distributions in $Mg(OH)_2$ precipitation from highly concentrated $MgCl_2$ solutions

G. Battaglia [a], S. Romano [a], A. Raponi [b], D. Marchisio [b], M. Ciofalo [a], A. Tamburini [a], A. Cipollina [a,*], G. Micale [a]

[a] Università degli studi di Palermo, Dipartimento di Ingegneria, Viale delle Scienze, 90128 Palermo, Italy
[b] Department of Applied Science and Technology, Institute of Chemical Engineering, Politecnico di Torino, Torino 10129, Italy

ARTICLE INFO

Article history:
Received 21 October 2021
Received in revised form 28 December 2021
Accepted 30 December 2021
Available online 05 January 2022

Keywords:
Magnesium hydroxide
Nanoparticles
Mixing
Precipitation
Reactive crystallization
Mineral recovery

ABSTRACT

Magnesium is a raw material of great importance, which attracted increasing interest in the last years. A promising route is to recover magnesium in the form of Magnesium Hydroxide via precipitation from highly concentrated Mg^{2+} resources, e.g. industrial or natural brines and bitterns. Several production methods and characterization procedures have been presented in the literature reporting a broad variety of $Mg(OH)_2$ particle sizes. In the present work, a detailed experimental investigation is aiming to shed light on the characteristics of produced $Mg(OH)_2$ particles and their dependence upon the reacting conditions. To this purpose, two T-shaped mixers were employed to tune and control the degree of homogenization of reactants. Particles were analysed by laser static light scattering with and without an anti-agglomerant treatment based on ultrasounds and addition of a dispersant. Zeta potential measurements were also carried out to further assess $Mg(OH)_2$ suspension stability.

1. Introduction

The growing energy, water and raw materials demand is the challenge that humankind is facing every day. In the novel and promising concept of circular economy, what has always been a waste becomes a valuable resource to be re-used and valorised.

Since ancient times, table salt has been harvested from the sea through saltworks. The process leads also to highly concentrated mineral solutions (bitterns), free of calcium, as a by-product. Bitterns represent a treasure chest of some crucial elements, e.g. magnesium (Mg), lithium (Li) and other trace elements (TE) [1].

Magnesium concentration is typically of 1.1 to 1.7 g/L in seawater and it can reach a value up to 60 g/L in bitterns. The magnesium market has risen sharply in recent years and is foreseen to considerably grow in the future [2]. Magnesium has also been listed among the 30 Critical Raw Materials for the European Union, due to the geographical distribution of its producers, which are mainly located in the USA, China and Russia [3].

Magnesium is widely employed in the form of magnesium hydroxide ($Mg(OH)_2$) and magnesium oxide (MgO). $Mg(OH)_2$ and MgO belong to a group of compounds with large numbers of favourable properties and possible practical applications [4]. Magnesium hydroxide is used as a flame-retardant filler in composite materials as it undergoes endothermic dehydration at high temperature, as an acidic waste neutralizer, as a pharmaceutical excipient, as a preservative in the pulp and paper industry, as a fertiliser additive, as a component in ethanol chemical sensors and as the most important precursor for the preparation of magnesium oxide, which is largely employed as a catalyst [4,5]. $Mg(OH)_2$ nanostructures have been obtained through several methods e.g. by microwave or ultrasonic/hydrothermal treatment [6,7], precipitation [1,8–12], precipitation with the aid of assistant additives [13], micro-emulsion method [14], bubbling set-up [15], hydrothermal process [16] and by means of a novel ionic exchange membrane crystallizer [17,18].

The recovery of magnesium from highly concentrated solutions represents a complex task. Turek et al. [11] successfully treated hard coal mine brine, which contained 2.84 g/L of magnesium, by extracting magnesium hydroxide through reactive precipitation. Cipollina et al. [1] produced high purity magnesium hydroxide from real bitterns collected from the saltworks operating in the district of Trapani (Italy). Yousefi et al. [10] synthetized magnesium hydroxide using poly(ethylene glycol, PEG 4000) as a surfactant; they applied a chemical precipitation method to an impure brine of the Khur Potash Complex's evaporation ponds (Isfahan, Iran). Vassallo et al. [19] presented a novel pilot plant for the selective recovery and removal of magnesium and calcium from retentate brines of a nanofiltration unit processing spent brines from the industrial water production plant of Evides Industriewater

* Corresponding author.
E-mail address: andrea.cipollina@unipa.it (A. Cipollina).

https://doi.org/10.1016/j.powtec.2021.117106

B.V. More than 90% of magnesium ions contained in the treated brine were recovered with magnesium hydroxide purities above 90%.

The above-cited authors investigated some effects of operating conditions on the final magnesium hydroxide features, such as sedimentation times or solids purity. However, the authors did not study the interaction between mixing and precipitation (or reactive crystallization) occurring during the whole process, which, in fact, significantly affect the characteristics of the produced particles.

The reactive crystallization process of $Mg(OH)_2$ is a complex mix of phenomena, involving mixing at all scales, including at the molecular scale (i.e. micro-mixing), chemical reaction and homogeneous and heterogeneous nucleation, molecular growth, aggregation and agglomeration. As mentioned, in the case of very fast crystallization kinetics, mixing has a crucial role in the control of the final produced particle characteristics and notable the size distribution. Magnesium hydroxide production from a highly concentrated solution represents an example of an extremely fast crystallization process. Many studies dealt with the characterization of the crystallization kinetics of $Mg(OH)_2$ [20–24]. Different experimental apparatuses were used, e.g. T-mixers [20] or stirred reactors [21,22]; the induction time (the period of time that elapses between the moment when supersaturated solutions are formed and the moment when precipitate appears) was found to be at most of the order of few seconds even when the magnesium concentration was as low as ~0.03 g/L [22].

Only a few works addressed the effect of mixing on the magnesium hydroxide precipitation processes from concentrated solutions. Shirure et al. [25] investigated the precipitation of magnesium hydroxide from magnesium chloride solutions (up to 24 g/L) using narrow channels T and Y- shaped mixers. The authors reported that at higher reactant flow rates, smaller $Mg(OH)_2$ particles were produced. The surfactant Tween 20 was added to the $Mg(OH)_2$ suspensions before particle size distributions (PSDs) measurements and the volume-average particle size was found to be from 5 μm to 30 μm. Song et al. [26] synthetized magnesium hydroxide particles with high purity by using $MgCl_2$ solutions (~40 g/L) and NaCl solution as assistant additive, in a glass reactor under vigorous stirring. In this case, PSDs were measured by static light scattering granulometry analysis without using surfactants and particles of the order of micrometres were reported. In addition, significant aggregate/agglomerates were observed by SEM images. Tai et al. [27] studied the precipitation of magnesium hydroxide nanoparticles from highly concentrated magnesium chloride solutions (up to 20 g/L) using a spinning disk reactor. The spinning disk reactor allowed a very good degree of mixing (a mixing time below 1 ms) leading to the synthesis of lamellar magnesium hydroxide particles of 50–80 nm length and 10 nm in thickness. In this case, the authors used a sonicator and poly(acrylic acid, sodium salt) (PAA) and sodium hexametaphosphate as dispersants. Particles were measured using a dynamic light scattering technology yielding number-average particle size from 40.0 to 47.5 nm. Shen et al. [28] developed a novel impinging stream-rotating packed bed reactor. In order to determine the particle size and distribution, the prepared samples were dispersed in distilled water by sonication for 10 min using a 2% sodium hexametaphosphate solution as a dispersant. Wide size distributions were found at low liquid flow rates and rotating packed bed speed, while PSDs narrowed when the liquid flow rates and the rotating packed bed speed increased (e.g. the increase of the fluid flow rate of a Mg^{2+} 18 g/L solution yielded a decrease of the volume-average size from 104 to 58.4 nm when the rotating packed bed velocity was 800 rpm).

The broad dispersed $Mg(OH)_2$ particle dimensions reported in the above-cited works mark the need for a deeper insight into the phenomena taking place during $Mg(OH)_2$ precipitation, including the undoubtful interaction between precipitation and mixing, the effect of ultrasounds and/or dispersant addition. To this aim, a comprehensive experimental study is here presented on the interaction between reactants mixing and $Mg(OH)_2$ precipitation from highly concentrated synthetic $MgCl_2$ solutions (Mg^{2+} 24 g/L). Two circular cross-sectional T-shaped mixers, having a diameter of 2 mm or 3 mm, were employed to tune and control the degree of reactants homogenization. PSDs were accessed using static light scattering technique, with and without ultrasounds treatment and addition of PAA as a dispersant. Also zeta potential measurements were conducted at different pH values in order to better investigate the tendency of particles to agglomerate.

To describe the state of particle assemblage, unfortunately, a broad disagreement is observed among different authors and sources on the definition of terms “agglomerates” and “aggregates” [29]. In the present paper the following definitions will be used:

- primary particles are single crystals or crystals composed of crystallites (or grain);
- aggregates are made of primary particles, which are united by strong chemical bonds that cannot be broken by fluid shear stresses and sonication;
- agglomerates are made of more or less loose arrangements of primary particles, aggregates or a mixture of the two held together by crystalline bridges or sometimes by electrostatic forces. Agglomerates are weaker than aggregates and can be separated by physical treatment such as sonication.

2. Materials and methods

2.1. Reactive crystallization stage

2.1.1. Experimental set up and $Mg(OH)_2$ reaction

A schematic representation of the employed experimental set-up is shown in Fig. 1. Magnesium hydroxide precipitation was carried out employing two circular-cross sectional T-mixers with a diameter of 2 and 3 mm, as shown in the insight of Fig. 1. The T-mixers were drilled in polymethyl methacrylate (PMMA) blocks and are constituted by two horizontal tracts (inlet channels) which merge into a vertical one (mixing channel). In both mixers, the inlet and mixing channels were of the same diameter (2 mm for mixer A and 3 mm for mixer B). The inlet channels were 10 times longer than the mixer diameter, i.e. 20 and 30 mm for mixers A and B, while the vertical channels were twenty times longer than the mixer diameter, i.e. 40 and 60 mm, respectively. The two T-mixers were employed to investigate the effect of mixing performance in the reactors on the precipitated $Mg(OH)_2$ particles. In particular, it is expected that narrower channels offer better mixing performance with respect to larger ones [30]. Magnesium chloride ($MgCl_2$) and sodium hydroxide (NaOH) solutions were pumped using two gear pumps (Fluid-o-Tech® FG series) controlled by dedicated software developed on LabView 2015.

Gear pumps are typically used for industrial applications, since they can be operated continuously, however they are not pulsation-free. The majority of the experiments reported here were conducted at high pump rotational speed, thus the effect of pulsation on the mixing of the reactants is expected to be negligible [31].

The chemical reaction involved in the formation of magnesium hydroxide is:

$$MgCl_2 + 2NaOH \rightarrow Mg(OH)_2 + 2NaCl \quad (1)$$

$MgCl_2$ and NaOH solutions were prepared by dissolving pellets of magnesium chloride hexahydrate for analysis (Sigma Aldrich) and NaOH (Honeywell FlukaTM, with an assay >98%) in ultrapure water. $MgCl_2$ concentrations were verified by Ionic Chromatography (Metrohm 882 compact IC plus), while NaOH concentrations were measured by titration. All solutions were prepared with an error in target concentration lower than 3% with respect to the desired values.

2.1.2. Flow rates and estimation of the characteristic mixing times

To design and scale-up precipitation reactors, it is important to estimate the mixing efficiencies and the characteristic mixing time attained

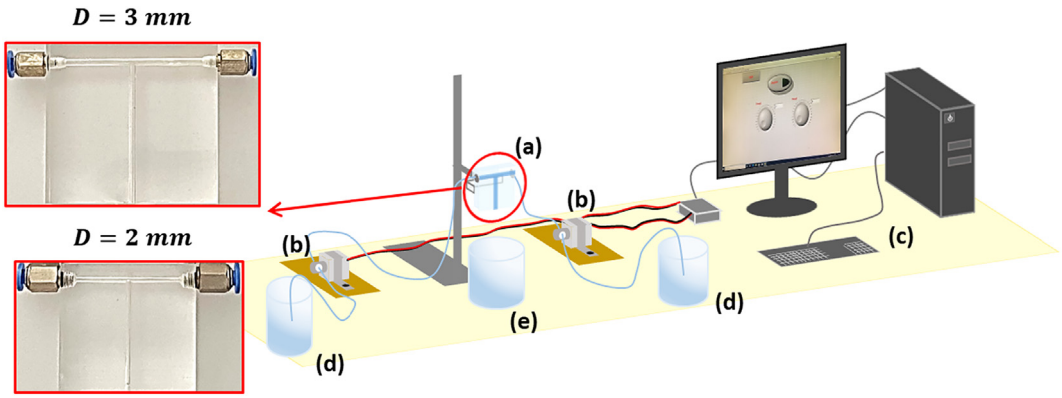

Fig. 1. Schematic representation of the employed experimental set-up: (a) T-mixer, (b) gear pumps, (c) computer for pumps control, (d) feed tanks, (e) discharge tank. On the left, an insight of the 3 and 2 mm T-mixers.

in the employed T-mixers. T-mixers are characterized by large area-to-volume ratio providing better mixing efficiencies with respect to conventional reactors (e.g. stirred reactors). In the last decades, T-mixers have been thoroughly investigated both experimentally [31,32] and numerically [30,33]. The characteristic mixing time (t_m) in such mixers depends on the specific definition adopted. However, an estimate is provided by Roelands et al. [30]:

$$t_m = \frac{12D}{v} \tag{2}$$

where D is the diameter of the vertical channel and v is the mean velocity in the same channel.

An alternative definition for mixing time in T-mixers has been recently proposed by Schikarski et al. [34]. The authors defined the mixing time taking into account the mixing homogeneity in the T-mixer based on a numerical/experimental study, comparing direct numerical simulation of the fluid flow to experimental Villermaux-Dushman characterization.

The effect of reactants homogenization, and thus of mixing time, on the precipitation of $Mg(OH)_2$ was investigated here at different fluid velocities in the mixing channel: from 0.6 ± 2% to 6.4 ± 2% m/s in the T-mixer of 3 mm diameter (mixing times between ~60 ms and ~6 ms); and from 4.1 ± 2% to 17 ± 2% m/s in the 2 mm diameter mixer (mixing times between ~6 ms and ~1 ms).

Table 1 lists all the cases investigated along with the flow rates, the mean velocity, the Reynolds number in the vertical channel and the estimation of the characteristic mixing times calculated using Eq. (2). In all cases, a 1 M $MgCl_2$ solution, a typical concentration of bitterns, was made to react with a stoichiometric 2 M solution of NaOH. $MgCl_2$ and NaOH solutions were fed at the same fluid flow rates, each half of the flow rate in the mixing channel. All tests were conducted at 25 °C.

Table 1
Geometrical and operating conditions of experimental tests. In all cases a 1 M $MgCl_2$ solution was made to react with a stoichiometric 2 M solution of NaOH. The flow rates, the mean velocity and the Reynolds numbers are calculated in the mixing channel.

Case	Mixer diameter **D** (mm)	Flow rate (mL/min)	Mean velocity **v** (m/s)	Reynolds number	Estimated mixing time (ms)
#1	3	260 ± 2%	0.6 ± 2%	2030	60
#2	3	460 ± 2%	1.1 ± 2%	3590	33
#3	3	1400 ± 2%	3.3 ± 2%	10,970	10
#4	3	2720 ± 2%	6.4 ± 2%	21,300	5.6
#5	2	780 ± 2%	4.1 ± 2%	9170	5.7
#6	2	1600 ± 2%	8.5 ± 2%	18,830	2.9
#7	2	2320 ± 2%	12 ± 2%	27,250	2.0
#8	2	3203 ± 2%	17 ± 2%	37,660	1.4

The Reynolds number was calculated as follows:

$$Re = \frac{\rho v D}{\mu} \tag{3}$$

where ρ and μ are the density and the viscosity of pure water at 25 °C (997 kg/m^3 and $0.89 \cdot 10^{-3}$ Pa·s, respectively), v is the mean fluid velocity in the vertical (mixing) channel and D is the channel diameter. The range of the investigated flow rates results in a range of Reynolds numbers from 2000 to 38,000.

The suspensions' pH was measured immediately after the outlet of the mixing channel. In all tests here presented, the measured pH values ranged between 10.3 and 10.6 (equilibrium pH of 10.48).

2.2. Product characterization stage

2.2.1. Particle size distribution measurements

$Mg(OH)_2$ particle size distributions (PSDs) were measured using a Malvern® Mastersizer 2000 granulometer with and without ultrasounds treatment and addition of a poly(acrylic acid, sodium salt), (PAA, MW 1200, Sigma-Aldrich, Inc.) as a dispersant.

The Mastersizer 2000 is a static light scattering equipment that uses a blue (488.0 μm wavelength LED) and red (633.8 μm wavelength He–Ne laser) light dual-wavelength, single-lens detection system. The light intensity adsorbed by particles is measured as obscuration and refers to the amount of the analysed sample. PSDs are obtained by processing light scattering data using the Malvern's Mastersizer 2000 software that employs either full Mie or Fraunhofer diffraction theories [35].

The granulometer was equipped with the Malvern® Hydro 2000 MU that uses a stirrer for the dispersion of the sample into ~800 mL of deionised water. All the analyses were carried out at stirrer velocity of 2000 rpm. This stirrer velocity was deemed to be the one that did not affect the obtained particle size distributions, after performing a preliminary stirrer speed influence study on PSDs as suggested in the literature [35–37]. The stirrer speed study was conducted to guarantee that small and big particles could be well suspended in the volume during all the measurement time, thus ensuring no particles sedimentation that could affect the obtained PSDs. Most Mastersizer2000 measurements were carried out as follows: (1) the PAA (when adopted) was added to water in the Hydro 2000 MU beaker (30 PAA drops for ~5 mL of $Mg(OH)_2$ 29.3 g/L suspension) and the background was measured; (2) the $Mg(OH)_2$ suspension was added until the light obscuration reached a value of ~24%; (3) at least 5 PSD measurements were conducted; (4) 5 min of ultrasounds treatment (sonication) were performed using the integrated ultrasound probe at 20 kHz; (5) at least 5 further PSD measurements were taken. For comparison

purposes, some PSD measurements were also conducted without either PAA or sonication. All $Mg(OH)_2$ samples were analysed within less than 15 min from their precipitation.

The effect of time delay in performing the analysis on the $Mg(OH)_2$ precipitation was investigated by quenching $Mg(OH)_2$ precipitates obtained from initial 0.1 M $MgCl_2$ and 0.2 M NaOH solutions. Specifically, the suspension exiting the T-mixer was quenched in a flask containing ultrapure water leading to a product dilution of 1:2 and 1:10. The collected solutions were then analysed by ionic chromatography to determine the final concentration of Mg^{2+} ions and thus Mg^{2+} conversion. In all cases, a total Mg^{2+} conversion was found suggesting that the reaction fully developed in the T-mixer; therefore, no effect (or a very low effect) of nucleation, particle growth and aggregation was expected after the solution exited the T-mixer. This is justified by the fact that supersaturation was already consumed even at these low concentrations, lower than those used in the actual tests (Table 1). Each experiment was repeated at least twice for the purpose of reproducibility.

2.2.2. Zeta potential measurements

In order to better understand the stability of $Mg(OH)_2$ colloids (the ability to stay in the colloidal form without particle agglomeration through flocculation [38]) and its implications on the obtained PSD, zeta potential measurements were conducted analysing $Mg(OH)_2$ suspensions produced: (i) after 2 h from the precipitation for Case #1 and Case #7 without PAA; (ii) after 1 month of aging for suspensions of Case #7 without PAA; (iii) after 2 h from the precipitation for Case #7 with PAA. The 2 h samples were analysed using a Malvern® Zetasizer Nano ZSP (analysis conducted at the Advanced Technologies Network Center of the University of Palermo), while the 1 month samples were analysed using a Malvern® Zetasizer Nano ZS90 (analysis conducted at Politecnico di Torino). All samples were diluted to a $Mg(OH)_2$ concentration of 0.3 g/L and drops of 1 M NaOH solution were added to adjust the suspensions pH to the desired one. It is worth mentioning that the value obtained for each measurement is the result of at least 12 repeated internal measurements of the Zetasizer, which eventually returns an average value with a standard deviation. Moreover, each experiment was repeated at least twice for reproducibility purposes. This allows to estimate the error bars reported in the results, by statistically combining the dispersion between different trials (reproducibility error) and the measurement error, provided for each individual trial by the device employed (Malvern Zetasizer).

2.2.3. SEM analysis

To investigate whether and how particles' morphology can be affected by precipitation conditions and post-treatment handling, $Mg(OH)_2$ particles morphology was analysed via Scanning Electron Microscopy (SEM FEI Quanta 200 FEG).

Morphologies were compared for Case #1 and Case#7 after performing two different particles preparation processes aiming at removing non-$Mg(OH)_2$ salts from the sample:

(i) $Mg(OH)_2$ suspensions were filtered by using a Büchner system and a vacuum pump; the cake was washed to remove the reaction-produced NaCl that remains trapped in the wet cake, then dried for 24 h in an oven at 120 °C and finally crashed by mortar & pestle.
(ii) 7 mL of $Mg(OH)_2$ suspension was added to 700 mL distilled water in the HydroMU 2000 beaker; 30 drops of PAA were added and 5 min of ultrasound treatment was applied; a drop of the diluted suspension was then withdrawn close to the impeller, positioned on a SEM stub and dried in a vacuum vessel for 48 h.

3. Results and discussion

3.1. Influence of the reactants mixing on the produced $Mg(OH)_2$ particles

In this section, the influence of mixing on the produced $Mg(OH)_2$ particles was assessed by comparing the PSDs obtained for the eight experimental conditions reported in Table 1. For the chosen concentrations of 1 M $MgCl_2$ and 2 M NaOH the minimum degree of mixing (the highest mixing time, see Eq. (2)) beyond which mixing has no further influence on particle formation was determined. As discussed in Section 2, PSDs were measured with and without ultrasounds treatment and addition of PAA in the characterization stage in order to assess the $Mg(OH)_2$ particle assemblage state.

3.1.1. $Mg(OH)_2$ PSDs without ultrasounds treatment and no addition of PAA

PSDs measurements were first performed without ultrasounds treatment and addition of PAA. The characteristic diameters dkm of the measured PSDs were calculated to study the effect of fluid flow regimes on the $Mg(OH)_2$ precipitation process. dkm denotes the ratio between the k-th and the m-th moments of the PSD:

$$dkm = \left[\frac{\int_0^\infty d^k n(d)\mathrm{d}d}{\int_0^\infty d^m n(d)\mathrm{d}d}\right]^{\frac{1}{k-m}} \tag{4}$$

where $n(d)$ is the number particle distribution function, such that $n(d)\,\mathrm{d}d$ is the number of particles having diameter between d and $d + \mathrm{d}d$. Thus, d10 is the number-average particle size more affected by small particles as they outnumber larger ones. Instead, d43 is the volume weighted-average particle size, which is more influenced by the presence of larger particles [39]. Fig. 2 reports the d43 and d10 characteristic diameters of the PSDs of the obtained $Mg(OH)_2$ precipitate for all the fluid flow regimes investigated as functions of Reynolds number, upper row, and the mixing time, lower row.

As can be seen in Fig. 2, neither d43 nor d10 exhibit a slightly influence of the Reynolds number or the diameter of the T-mixers. In particular, d43 decreases from 30 to 10 μm when the 3 mm diameter T-mixer is used (solid symbols in Fig. 2.a), while it fluctuates around 20 μm in the case of the 2 mm diameter T-mixer (hollow symbols in Fig. 2.a). d10 decreases from ~6 μm to ~3 μm when the flow rate increases in both mixers (Fig. 2.b). These results were somehow un-expected, as in previous works the characteristic dimension of the particles was reported to decrease and PSDs to become more narrow as the mixing of reactants increased, as in the case of barium sulphate [39–41].

For the sake of completeness, volume-particle size distribution (V-PSD) of all the investigated Cases are also illustrated in Fig. 3. In particular, V-PSD reports the quantity $\varphi(d)$, which is the volume particle distribution function normalized by the total volume of particles, such that $\varphi(d)\mathrm{d}d$ is the volume percent of particles having diameters between d and $d + \mathrm{d}d$.

V-PSDs show a rather random influence either of mixing reactants flow rate or T-mixer diameter. The obtained $Mg(OH)_2$ V-PSDs are of the same order of particle dimensions with respect to those reported by Song et al. [26] and Shirure et al. [25]. Note that also the latter authors produced $Mg(OH)_2$ and did not treat particles with ultrasounds and adding dispersants (see further remarks at the end of Section 3.2).

3.1.2. $Mg(OH)_2$ particle size distributions with PAA and ultrasounds

Particle size distributions were also investigated after ultrasounds treatment and the addition of PAA. The use of PAA was used by several other authors [38,42,43]. Fig. 4 reports the obtained d43 and d10 for the same cases of Fig. 2 as functions of Reynolds number, upper row, and the mixing time, lower row.

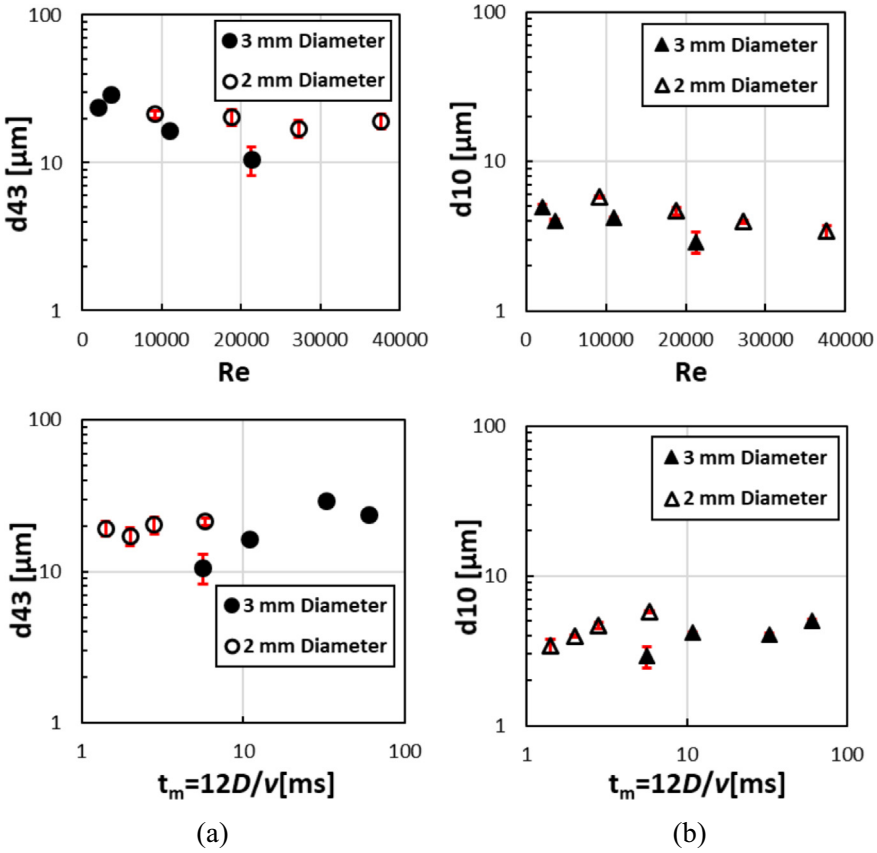

Fig. 2. Characteristic diameters of $Mg(OH)_2$ particles obtained using T-mixers with a diameter of 3 mm (solid symbols) or 2 mm (hollow symbols) as functions of Reynolds number, upper row, and mixing time, lower row: a) d43; b) d10. No sonication or PAA treatment was performed.

Particle sizes significantly differ from those reported in Fig. 2 and a stronger, although still irregular, influence of mixing parameters (velocity and diameters) on the characteristic particle diameters can be now observed. In particular, d43 (Fig. 4.a) decreases from ~5 μm to ~1 μm when the Reynolds number increases from ~2000 to ~20,000 in the 3 mm diameter T-mixer. Lower d43 values are observed for all the fluid flow rates when the 2 mm diameter T-mixer is employed, indicating a better mixing quality. Specifically, d43 values decrease from ~1 μm at *Re* of ~10,000 to ~0.1 μm at *Re* of ~27,000–38,000 (Cases #7 and #8). In the 3 mm diameter T-mixer, d10 (Fig. 4.b) increases for Reynolds numbers <10,000, while it suddenly drops at the investigated highest Reynolds value (i.e. ~20,000). The 2 mm diameter T-mixer guarantees better mixing quality as d10 exhibits low values even at the lowest fluid flow rate and settles at ~0.08 μm at Reynolds number of ~27,000–38,000 (Case #7 and #8).

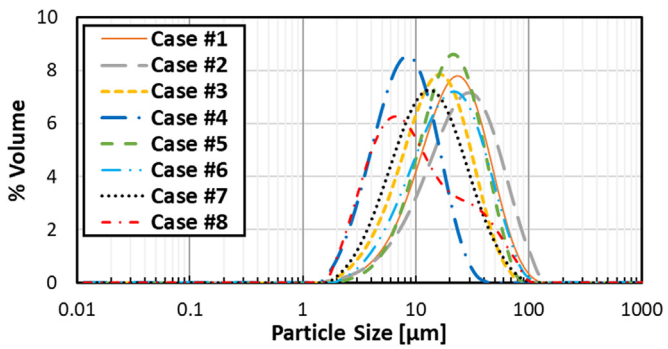

Fig. 3. Volume particle size distributions for all the investigated Cases. No sonication or PAA treatment was performed. Cases #1–4 are obtained in the 3 mm diameter T-mixer, while cases #5–8 in the 2 mm diameter (Table 1).

The volume-PSDs for all Cases are shown in Fig. 5.

From Case #4 to Case #6, i.e. for intermediate mixing intensities (mixing times between 6 and 3 ms), V-PSDs are bi-modal distributions with two peaks, one at ~2.7 μm for coarse particles and another at ~0.13 μm for fine particles. Such bi-modal distributions are typical of *shattering*, probably caused by the use of ultrasounds, by which large agglomerates are broken into aggregates (the fine particles having peak size ~0.13 nm) and smaller agglomerates (exhibiting a peak size of ~2.7 μm) [44]. The total volume of larger agglomerates decreases, and the total volume of the smaller aggregates increases as mixing increases, while peak particle sizes remain almost the same. On the other hand, from Case #1 to Case#3 (high mixing times ranging from 60 to 10 ms), V-PSDs indicate a unimodal distribution with the presence of mainly coarse particles, whose size is 2–3 times smaller than those shown in Fig. 3. Finally, at the highest mixing rate (mixing time values lower than 2 ms), Cases #7 and #8, particles are again monodispersed exhibiting only one peak at ~0.13 μm, characteristic of $Mg(OH)_2$ aggregates. It should be worth to recall that, in the present work, the term aggregates refers to primary particles, which are made of crystals united by strong chemical bonds and cannot be broken by fluid shear stresses and sonication. On the other side, the term agglomerates refers to looser or stronger arrangements of primary particles, aggregates, or a mixture of the two, held together by crystalline bridges or sometimes by electrostatic forces. Agglomerates are weaker than aggregates and can be separated by physical treatment such as sonication.

A possible explanation of the behaviour exhibited by the above discussed results lies in the interaction between mixing and the numerous phenomena involved in the precipitation process, as discussed by many

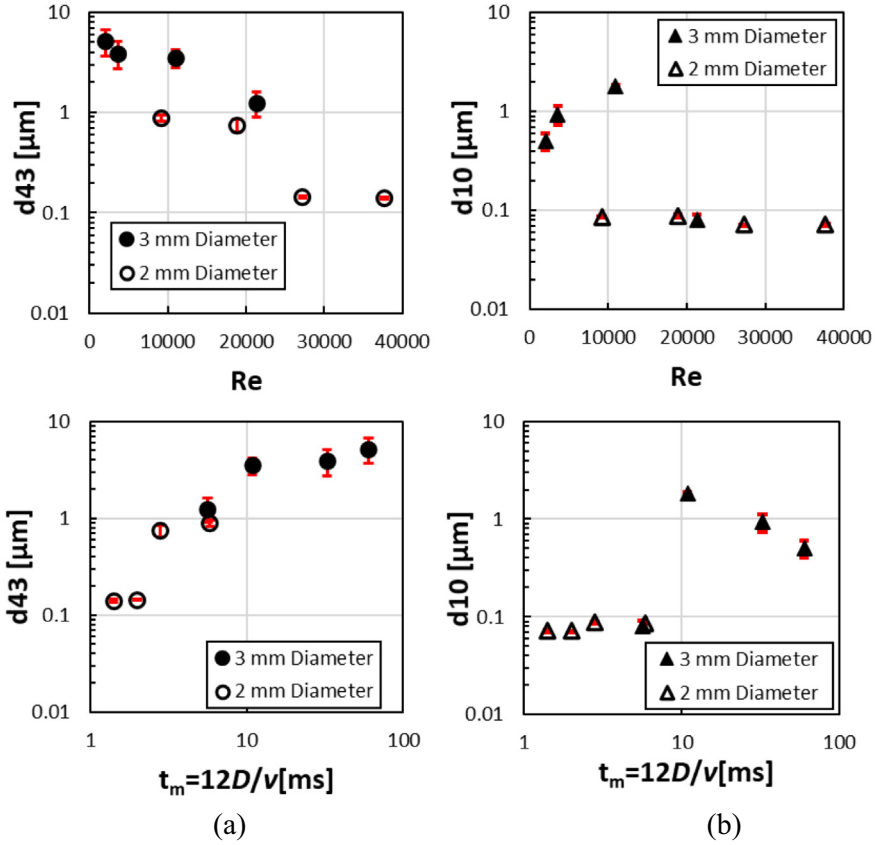

Fig. 4. Characteristic diameters of $Mg(OH)_2$ particles obtained using T-mixers with a 3 mm (solid symbols) or 2 mm (hollow symbols) as functions of the Reynolds number, upper row, and mixing time, lower row: a) d43; b) d10. PSDs were obtained after 5 min of ultrasounds treatment and using PAA as a dispersant.

authors [45,46]. Larger particles are produced in the reactive stage when mixing is poor (high mixing times) due to the combination of (1) a low homogenization degree of the reactants, yielding high local supersaturation levels, and (2) large and long-lived Kolmogorov eddies, which can enclose a high number of particles that can remain close to one another enough time to establish strong bridges between them. These bridges cannot be broken by the low fluid shear stresses. Conversely, at high Reynolds numbers, mixing becomes more efficient (low mixing times); more homogenous supersaturation is attained; small and short-lived Kolmogorov eddies are formed, so that a lower number of particles are entrapped inside each eddy, and stay together for a shorter time. These particles could form either small aggregates or weak agglomerates, the latter characterized by bridges which could be broken by the high fluid shear stresses.

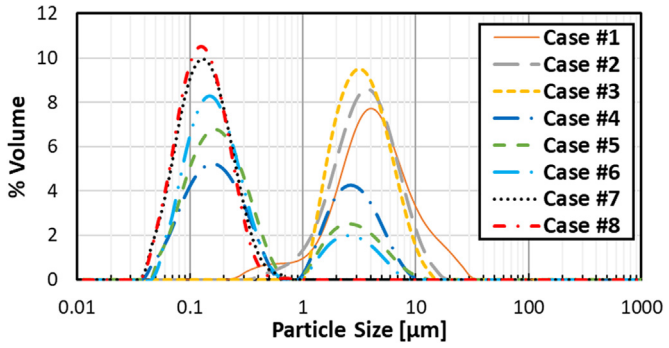

Fig. 5. Volume particle size distributions for all the investigated Cases. V-PSDs were obtained after 5 min of ultrasounds treatment and using PAA as a dispersant. Cases #1–4 are obtained in the 3 mm diameter T-mixer, while cases #5–8 in the 2 mm diameter (Table 1).

For the presented results (Fig. 5), it can be stated that a mixing time of at most 2 ms (Cases #7 and #8) must be achieved inside the reactor in order to well homogenize highly concentrated $MgCl_2$ (1 M) and NaOH (2 M) solutions. As a matter of fact, $Mg(OH)_2$ nanoparticles produced for Cases #7 and #8 (mixing times lower than ~2 ms) are characterized by aggregates or weak agglomerates, the latter breakable by the use of ultrasounds, leading to aggregates of ~100–200 nm after sonication. Similar PSDs are obtained in these two cases since, in reactive crystallization, homogeneous primary nucleation of particles is the main crystallization mechanism characterizing the process. At the same time, particle growth and aggregation occur. All these mechanisms are ruled by the supersaturation level in the system. When mixing does not represent the rate-limiting step and homogenous supersaturation is attained, particle size distributions only depend on nucleation, particle growth and particle aggregation characteristic of the specific precipitation process. These, in their turn, mainly depend on the supersaturation at the given reactants concentration, which was the same in cases #7 and #8. On the contrary, $Mg(OH)_2$ nanoparticles produced for Cases #1–3 (mixing times between 60 and 10 ms) are characterized by strong agglomerates, which require high energy to be broken into aggregates, thus exhibiting V-PSDs of micrometre sized agglomerates after 5 min of sonication due to a low mixing of the reactants. The intermediate mixing rates of Cases #4–6 (mixing times between ~6 ms and ~3 ms), instead, consist of a mix of strong and weak agglomerates, which can be partially broken to aggregates by ultrasounds leading to a bi-modal distribution characterized by aggregates of ~100–200 nm and agglomerates having a peak size of ~2.7 µm.

The importance of mixing time as a controlling parameter is also confirmed by the fact that suspensions produced using different T-

mixers (3 and 2 mm diameter for Case #4 and Case#5) and flow rates (2720 and 780 mL/min for Case #4 and Case #5), but having similar mixing times (~6 ms) exhibit similar V-PSDs (see Fig. 5) and particle size dimensions, as clearly shown in the lower row of Fig. 4.

$Mg(OH)_2$ nanoparticles obtained for Case #7 and 8 at a mixing time lower than ~2 ms have comparable particle dimensions with those reported by Tai et al. [27], i.e. d10 ~ 60 nm, who also produced $Mg(OH)_2$ nanoparticles starting from 1 M $MgCl_2$ employing a spinning disk reactor where the mixing time was reported to be of ~1 ms.

3.2. Zeta potential measurements

In Section 3.1 it was shown that particle size distributions significantly vary when suspensions are treated by using ultrasounds and adding PAA as a dispersant. In order to better understand these results, the effect of superficial electric charge of $Mg(OH)_2$ particles was examined by performing Zeta-potential measurements. The stability of $Mg(OH)_2$ suspensions was also investigated over time performing the analysis (i) after 2 h and (ii) after 1 month of aging from the precipitation. Zeta-potential depends on the particle properties, the suspension conditions (e.g. pH), and the theoretical model applied, e.g. the Smoluchowski approximation employed here to derive Zeta-potential values from the electrophoretic mobility of particles [47]. Fig. 6 a presents Zeta-potential values measured for Case #1 and Case #7 (see Table 1) after 2 h from the precipitation and for Case #7 after 1 month from precipitation for suspension pH ranging from 10 to 13, as described in Section 2.2.2. Fig. 6 b shows a comparison between Zeta potential measurements for Case #7 (2 h samples) with and without the addition of PAA.

The experimental data collected in this study was compared with those presented by Lin et al. [48]. The latter authors employed an electro-acoustic technique, while the data reported here were obtained by means of Malvern® Zetasizers, which are based on the electrophoretic mobility technique, i.e. on measuring the limiting velocity of the particles in an electric field.

At solution pH between 10 and 11, a good agreement is observed between Lin et al. data and Zeta-potential values measured analysing the 2 h samples of Case #7. Aged samples and those obtained for Case #1 showed an even better agreement with the measurements of Lin et al.

Specifically, Zeta-potential values measured for Case #7 (2 h samples) were found to vary from ~19 mV to ~18 mV as pH values varied from 10 to 11, while Zeta-potential values reported by Lin et al. and those measured for the aged samples and Case #1 (2 h samples) decreased from ~22 mV to ~20 mV. Some difficulties were encountered for measurements in high pH suspensions due to their high conductivity values, so that pH values higher than 12.5 could not be investigated. Lin et al., however, reported Zeta-potential values of ~ -15 mV at pH ~12.5 and ~ -20 mV at pH ~ 13. The isoelectric point (the point of zero Zeta-potential, where colloids have the largest tendency to agglomerate) of $Mg(OH)_2$ particles is detected at a pH value of ~12 for both 2 h samples and aged samples, in good agreement with Lin et al. and with values reported in literature [43,49,50].

Zeta-potential values measured for samples produced after 2 h from precipitation, both for Case#1 and Case #7, and those aged for 1 month show that $Mg(OH)_2$ suspensions are characterized by the same stability characteristics over time and similar Zeta potential values. Therefore, no influence on the Zeta potential value can be observed at different mixing conditions. From Fig. 6, it can be clearly seen that the Zeta-potential of the $Mg(OH)_2$ particles lies in the range of $\pm$30 mV, which represents a zeta potential region were particles are not stable and tend to agglomerate rather than staying apart [47]. These Zeta-potential values explain the behaviour shown in Section 3.1. Specifically, in the absence of PAA, $Mg(OH)_2$ particles agglomerate due to their low zeta potential values. On the other hand, the presence of PAA stabilizes the $Mg(OH)_2$ suspension [38,42], as clearly shown in Fig. 6 b. Specifically, the addition of the PAA causes an increases of the Zeta potential that reaches values of 35–40, in absolute value, away from the $\pm$30 mV unstable Zeta potential region, which is the expected effect of PAA surrounding the particles and modifying their zeta-potential and agglomeration tendency.

The thermodynamically stable coiled structure of PA^- can entrap $Mg(OH)_2$ nanoparticles preventing their agglomeration [38]. Thus, V-PSDs obtained in the absence of sonication and no PAA addition, as in Fig. 3, do not exhibit a significant influence of mixing in the reactive crystallization stage because they mainly regard the size distribution of large and weak agglomerates with typical peak dimensions in the 8–20 μm range. On the contrary, V-PSDs obtained by applying sonication and PAA treatment (Fig. 5) exhibit a much larger influence of the mixing intensity experienced in the reactive crystallization stage; for low mixing, V-PSDs exhibit agglomerates smaller than those in Fig. 3, but still characterized by peak size of 2-3 μm, while, for high mixing, they only consist of aggregates with a typical size of 100–200 nm.

3.3. Tyndall effect and $Mg(OH)_2$ particles morphology

The reduction of the particles sizes presented in Fig. 4 with respect to those reported in Fig. 3 was also confirmed by a visual inspection of the $Mg(OH)_2$ suspension contained in the Hydro 2000 MU beaker, as shown

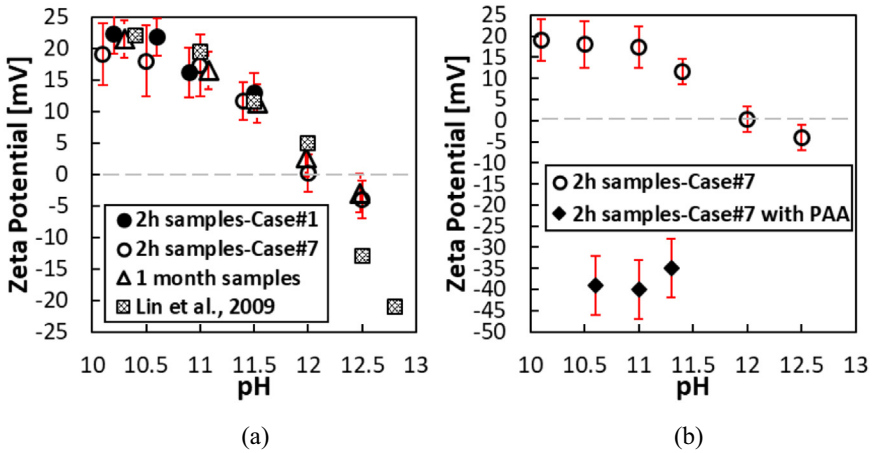

Fig. 6. $Mg(OH)_2$ Zeta potential values as functions of suspension pH: (a) circle symbols refer to 2 h samples (Case #1 bold circles and Case #7 hollow circles) and hollow triangles refer to 1 month aged $Mg(OH)_2$ suspensions. Lin et al. data (square symbols) were taken from [48]. (b) A comparison between Zeta potential values of $Mg(OH)_2$ suspensions produced under the mixing conditions of Case #7 (i) without PAA (hollow circles, 2 h samples) and (ii) with PAA (bold rhombus, 2 h samples).

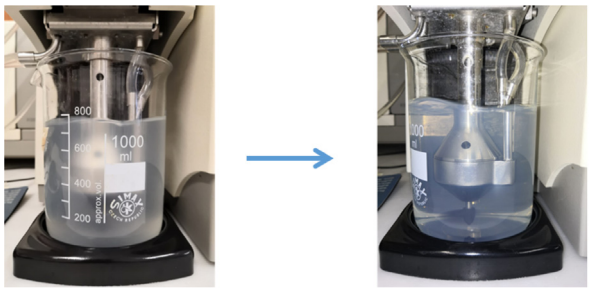

Fig. 7. $Mg(OH)_2$ suspensions in the Malvern® Hydro 2000 MU beaker before (a) and after (b) applying ultrasounds in the presence of PAA for Case #7 and Case #8. The blueish colour of the suspension after the anti-agglomerant treatment (b) indicates the presence of particles with dimensions below ~900 nm (Tyndall effect).

in Fig. 7 for Case #7 and Case #8. The $Mg(OH)_2$ suspension changes from a whitish to a blue colour due to the Tyndall effect. The Tyndall effect occurs when light is scattered by particles with diameters below ~900 nm [51], demonstrating the presence of nanometre sized particles in the beaker. Contrariwise, suspensions of particles produced under conditions #1–6 did not exhibit Tyndall effect due to the fact that the presence of large particles dominate and mask the effect of small particles. Note that, when measuring nanometre $Mg(OH)_2$ particles, the absorption value of $Mg(OH)_2$ was changed from 0.1 to 0.

As far as the morphology of the $Mg(OH)_2$ particles is concerned, Fig. 8 presents a comparison between four SEM images, at the same magnification (50,000×), of $Mg(OH)_2$ particles for Case #1 (Fig. 8 a, c) and for Case #7 (Fig. 8 b, d) after particles filtration and drying in an oven (Fig. 8 a, b) or after dilution and drying in a vacuum evaporator (Fig. 8 c, d), as described in Section 2.2.3. Globular $Mg(OH)_2$ nanometric particles with characteristic sizes of ~50–100 nm can be observed in all the SEM images. Comparing Fig. 8 a and b or Figures c and d, it can be seen that $Mg(OH)_2$ particles morphology is not affected by the different mixing regimes of Case #1 and Case #7, as particles are very similar in size and shape in the two investigated cases. On the other hand, the particle preparation process slightly affects the $Mg(OH)_2$ particles morphology. $Mg(OH)_2$ particles, in fact,

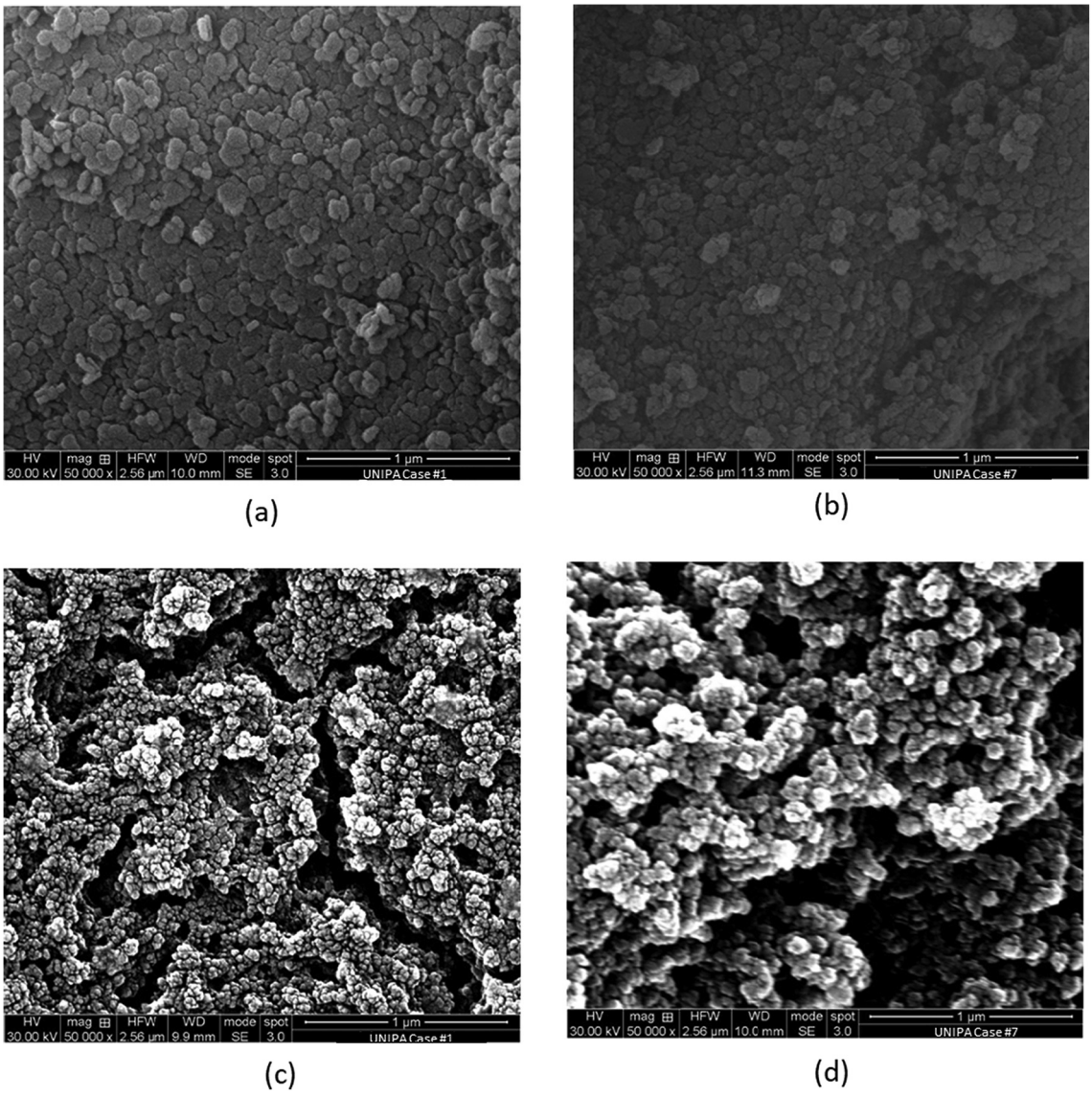

Fig. 8. SEM images of produced $Mg(OH)_2$ particles at a magnification of 50,000× for: (a, c) Case #1; (b, d) Case #7. Particles were prepared for SEM analysis: (a, b) after suspension filtration and drying in an oven; (c, d) after dilution and drying in a vacuum vessel.

show a tendency to exhibit a platelet-like morphology after the filtration and the oven drying treatment, while this tendency is not observed for particles obtained by the dilution and vacuum drying process. Similar particles morphologies as in Fig. 8 a and b were also reported in the literature for $Mg(OH)_2$ particles produced by precipitation using $MgCl_2$ solutions [43,52].

4. Conclusions

The precipitation process of magnesium hydroxide from 1 M $MgCl_2$ solutions was experimentally investigated focusing on the effect of reactants mixing on particle size distribution by a clearly methodical analytical procedure for the characterization of the produced $Mg(OH)_2$ particles. Two circular cross-sectional T-shaped mixers of 2 and 3 mm diameter were employed. Eight different cases were investigated with variable flow rates and channel diameter, in the range of Reynolds numbers between 2000 and 38,000, thus leading to mixing times ranging from 60 to 1.5 ms. Produced particles were analysed via a light scattering technique within 15 min from precipitation, with and without sonication (ultrasounds treatment) and poly(acrylic acid sodium salt) (PAA) addition.

It was found that in the absence of PAA and ultrasounds treatment particles could not be well characterized since similar V-PSDs exhibiting large agglomerates with peak sizes of 8–20 μm were detected for all the cases investigated. On the contrary, by using PAA and sonication, the effect of reactants mixing was clearly shown and the particles assemblage state well characterized. Specifically, for intermediate mixing regimes, V-PSDs were found to be bi-modal with two peaks, one at ~2.7 μm characteristic of small $Mg(OH)_2$ agglomerates and another at ~0.13 μm characteristic of $Mg(OH)_2$ aggregates. At low mixing rates, V-PSDs indicated a unimodal distribution with the presence of only agglomerates exhibiting a peak of ~2.7 μm, while at the highest mixing, when mixing time reaches values below 2 ms, particles were again monodispersed, exhibiting only one peak size of ~0.13 μm, representative of $Mg(OH)_2$ aggregates.

Results suggest that the use of T-mixers or other reactors ensuring similarly short mixing times should be employed for the production of nanoparticles $Mg(OH)_2$, whose characteristics have attracted much interest in the industrial field.

The similar V-PSDs obtained without any particle treatment were consistent with the low measured zeta potential values of the $Mg(OH)_2$ particles, which were found to lie in the range of ± 30 mV, marking a high tendency of particles to agglomerate due to electrostatic forces.

Declaration of Competing Interest

The authors declare that they have no known competing financial interests or personal relationships that could have appeared to influence the work reported in this paper.

Acknowledgments

This project has received funding from the European Union's Horizon 2020 Research and Innovation Programme under Grant Agreement No. 869467 (SEArcularMINE). This output reflects only the author's view. The European Health and Digital Executive Agency (HaDEA) and the European Commission cannot be held responsible for any use that may be made of the information contained therein. Authors are grateful to Simone Bonafede for having contributed to this work during his master thesis.

References

[1] A. Cipollina, M. Bevacqua, P. Dolcimascolo, A. Tamburini, A. Brucato, H. Glade, L. Buether, G. Micale, Reactive crystallisation process for magnesium recovery from concentrated brines, Desalin. Water Treat. 55 (2015) 2377–2388, https://doi.org/10.1080/19443994.2014.947771.

[2] Magnesium Metal Outlook to 203013th edition, 2021 1–7 https://roskill.com/market-report/magnesium-metal/.

[3] Critical Raw Materials Resilience: Charting a Path towards Greater Security and Sustainability, https://eur-lex.europa.eu/legal-content/EN/TXT/PDF/?uri=CELEX:52020DC0474&from=EN 2020.

[4] A.A. Pilarska, Ł. Klapiszewski, T. Jesionowski, Recent development in the synthesis, modification and application of Mg(OH)2 and MgO: a review, Powder Technol. 319 (2017) 373–407, https://doi.org/10.1016/j.powtec.2017.07.009.

[5] G. Balducci, L. Bravo Diaz, D.H. Gregory, Recent progress in the synthesis of nanostructured magnesium hydroxide, CrystEngComm 19 (2017) 6067–6084, https://doi.org/10.1039/c7ce01570d.

[6] H.Y. Zahran, S.S. Shneouda, I.S. Yahia, F. El-Tantawy, Facile and rapid synthesis of nanoplates Mg(OH)2 and MgO via microwave technique from metal source: structural, optical and dielectric properties, J. Sol-Gel Sci. Technol. 86 (2018) 104–111, https://doi.org/10.1007/s10971-018-4613-2.

[7] W. Shu-Yu, H. Wen-Zhi, L. Chang, L. Guang-Ming, Z. Fei-Er, Characterizations and preparation of Mg(OH)2 nanocrystals through ultrasonic–hydrothermal route, Res. Chem. Intermed. 42 (2016) 4135–4145, https://doi.org/10.1007/s11164-015-2264-2.

[8] J. Zheng, W. Zhou, Solution-phase synthesis of magnesium hydroxide nanotubes, Mater. Lett. 127 (2014) 17–19, https://doi.org/10.1016/j.matlet.2014.04.076.

[9] A. Alamdari, R.M. Rahimpour, N. Esfandiari, E. Nourafkan, Kinetics of magnesium hydroxide precipitation from sea bittern, Chem. Eng. Process. Process Intensif. 47 (2008) 215–221, https://doi.org/10.1016/j.cep.2007.02.012.

[10] S. Yousefi, B. Ghasemi, M. Tajally, PEG-assisted synthesis and formation mechanism of Mg(OH)2 nanostructures using natural brine, Appl. Phys. A Mater. Sci. Process. 126 (2020) https://doi.org/10.1007/s00339-020-03814-w.

[11] M. Turek, W. Gnot, Precipitation of magnesium hydroxide from brine, Ind. Eng. Chem. Res. 34 (1995) 244–250, https://doi.org/10.1021/ie00040a025.

[12] A. Pilarska, M. Wysokowski, E. Markiewicz, T. Jesionowski, Synthesis of magnesium hydroxide and its calcinates by a precipitation method with the use of magnesium sulfate and poly(ethylene glycols), Powder Technol. 235 (2013) 148–157, https://doi.org/10.1016/j.powtec.2012.10.008.

[13] J.P. Hsu, A. Nacu, Preparation of submicron-sized Mg(OH)2 particles through precipitation, Colloids Surf. A 262 (2005) 220–231, https://doi.org/10.1016/j.colsurfa.2005.04.038.

[14] H. Wu, B. Luo, C. Gao, L. Wang, Y. Wang, Q. Zhang, Synthesis and size control of monodisperse magnesium hydroxide nanoparticles by microemulsion method, J. Dispers. Sci. Technol. 41 (2020) 585–591, https://doi.org/10.1080/01932691.2019.1594887.

[15] X. Li, C. Ma, J. Zhao, Z. Li, S. Xu, Y. Liu, Preparation of magnesium hydroxide nanoplates using a bubbling setup, Powder Technol. 198 (2010) 292–297, https://doi.org/10.1016/j.powtec.2009.11.024.

[16] D. Wang, C. Song, Z. Hu, Synthesis of mono-dispersed Mg(OH)2 nanoflakelets, J. Dispers. Sci. Technol. 29 (2008) 1010–1012, https://doi.org/10.1080/01932690701810011.

[17] D. La Corte, F. Vassallo, A. Cipollina, M. Turek, A. Tamburini, G. Micale, A novel ionic exchange membrane crystallizer to recover magnesium hydroxide from seawater and industrial brines, Membranes (Basel) 10 (2020) 1–14, https://doi.org/10.3390/membranes10110303.

[18] F. Vassallo, C. Morgante, G. Battaglia, D. La Corte, M. Micari, A. Cipollina, A. Tamburini, G. Micale, A simulation tool for ion exchange membrane crystallization of magnesium hydroxide from waste brine, Chem. Eng. Res. Des. (2021) https://doi.org/10.1016/j.cherd.2021.07.008.

[19] F. Vassallo, D. La Corte, N. Cancilla, A. Tamburini, M. Bevacqua, A. Cipollina, G. Micale, A pilot-plant for the selective recovery of magnesium and calcium from waste brines, Desalination 517 (2021) https://doi.org/10.1016/j.desal.2021.115231.

[20] S. Bhandarkar, R. Brown, J. Estrin, Studies in rapid precipitation of hydroxides of calcium and magnesium, J. Cryst. Growth 97 (1989) 406–414, https://doi.org/10.1016/0022-0248(89)90222-4.

[21] D.J. Gunn, M.S. Murthyt, M.S. Murthy, Kinetics and mechanisms of precipitations, Chem. Eng. Sci. 27 (1972) 1293–1313, https://doi.org/10.1016/0009-2509(72)80105-2.

[22] Q. Yuan, Z. Lu, P. Zhang, X. Luo, X. Ren, T.D. Golden, Study of the synthesis and crystallization kinetics of magnesium hydroxide, Mater. Chem. Phys. 162 (2015) 734–742, https://doi.org/10.1016/j.matchemphys.2015.06.048.

[23] A.E. Nielsen, O. Söhnel, Interfacial tensions electrolyte crystal-aqueous solution, from nucleation data, J. Cryst. Growth 11 (1971) 233–242, https://doi.org/10.1016/0022-0248(71)90090-X.

[24] A. Packter, The rapid precipitation of magnesium hydroxide from aqueous solutions: analysis of nucleation and crystal growth kinetics, final nucleus numbers and primary crystal sizes, Cryst. Res. Technol. 20 (1985) 329–336, https://doi.org/10.1002/crat.2170200307.

[25] V.S. Shirure, A.S. Pore, V.G. Pangarkar, Intensification of precipitation using narrow channel reactors: magnesium hydroxide precipitation, Ind. Eng. Chem. Res. 44 (2005) 5500–5507, https://doi.org/10.1021/ie049248d.

[26] X. Song, S. Sun, D. Zhang, J. Wang, J. Yu, Synthesis and characterization of magnesium hydroxide by batch reaction crystallization, Front. Chem. Sci. Eng. 5 (2011) 416–421, https://doi.org/10.1007/s11705-011-1125-9.

[27] C.Y. Tai, C. Te Tai, M.H. Chang, H.S. Liu, Synthesis of magnesium hydroxide and oxide nanoparticles using a spinning disk reactor, Ind. Eng. Chem. Res. 46 (2007) 5536–5541, https://doi.org/10.1021/ie060869b.

[28] H. Shen, Y. Liu, B. Song, Preparation and characterization of magnesium hydroxide nanoparticles in a novel impinging stream-rotating packed bed reactor, J. Chem. Eng. Jpn. 49 (2016) 372–378, https://doi.org/10.1252/jcej.15we093.

[29] G. Nichols, S. Byard, M.J. Bloxham, J. Botterill, N.J. Dawson, A. Dennis, V. Diart, N.C. North, J.D. Sherwood, A review of the terms agglomerate and aggregate with a recommendation for nomenclature used in powder and particle characterization, J. Pharm. Sci. 91 (2002) 2103–2109, https://doi.org/10.1002/jps.10191.
[30] M. Roelands, J. Derksen, J. ter Horst, H. Kramer, P. Jansens, An analysis of mixing in a typical experimental setup to measure nucleation rates of precipitation processes, Chem. Eng. Technol. 26 (2003) 296–303, https://doi.org/10.1002/ceat.200390045.
[31] C. Lindenberg, J. Schöll, L. Vicum, M. Mazzotti, J. Brozio, Experimental characterization and multi-scale modeling of mixing in static mixers, Chem. Eng. Sci. 63 (2008) 4135–4149, https://doi.org/10.1016/j.ces.2008.05.026.
[32] S. Romano, G. Battaglia, S. Bonafede, D. Marchisio, M. Ciofalo, A. Tamburini, A. Cipollina, G. Micale, Experimental assessment of the mixing quality in a circular cross-sectional T-shaped mixer for the precipitation of sparingly soluble compounds, Chem. Eng. Trans. (2021) 1165–1170, https://doi.org/10.3303/CET2186195.
[33] D. Bothe, C. Stemich, H.J. Warnecke, Fluid mixing in a T-shaped micro-mixer, Chem. Eng. Sci. 61 (2006) 2950–2958, https://doi.org/10.1016/j.ces.2005.10.060.
[34] T. Schikarski, H. Trzenschiok, W. Peukert, M. Avila, Inflow boundary conditions determine T-mixer efficiency, React. Chem. Eng. 4 (2019) 559–568, https://doi.org/10.1039/c8re00208h.
[35] F. Storti, F. Balsamo, Particle size distributions by laser diffraction: sensitivity of granular matter strength to analytical operating procedures, Solid Earth 1 (2010) 25–48, https://doi.org/10.5194/se-1-25-2010.
[36] M. Ryzak, A. Bieganowski, Methodological aspects of determining soil particle-size distribution using the laser diffraction method, J. Plant Nutr. Soil Sci. 174 (2011) 624–633, https://doi.org/10.1002/jpln.201000255.
[37] M. Sperazza, J.N. Moore, M.S. Hendrix, High-resolution particle size analysis of naturally occurring very fine-grained sediment through laser diffractometry, J. Sediment. Res. 74 (2004) 736–743, https://doi.org/10.1306/031104740736.
[38] M.G.P.G. Mantilaka, H.M.T.G.A. Pitawala, D.G.G.P. Karunaratne, R.M.G. Rajapakse, Nanocrystalline magnesium oxide from dolomite via poly(acrylate) stabilized magnesium hydroxide colloids, Colloids Surf. A 443 (2014) 201–208, https://doi.org/10.1016/j.colsurfa.2013.11.020.
[39] D.L. Marchisio, L. Rivautella, A.A. Barresi, Design and scale-up of chemical reactors for nanoparticle precipitation, AICHE J. 52 (2006) 1877–1887, https://doi.org/10.1002/aic.10786.
[40] M. Kucher, D. Babic, M. Kind, Precipitation of barium sulfate: experimental investigation about the influence of supersaturation and free lattice ion ratio on particle formation, Chem. Eng. Process. Process Intensif. 45 (2006) 900–907, https://doi.org/10.1016/j.cep.2005.12.006.
[41] H.C. Schwarzer, W. Peukert, Combined experimental/numerical study on the precipitation of nanoparticles, AICHE J. 50 (2004) 3234–3247, https://doi.org/10.1002/aic.10277.
[42] K. Tong, X. Song, G. Xiao, J. Yu, Colloidal processing of Mg(OH)2 aqueous suspensions using sodium polyacrylate as dispersant, Ind. Eng. Chem. Res. 53 (2014) 4755–4762, https://doi.org/10.1021/ie5002857.
[43] C. Henrist, J.P. Mathieu, C. Vogels, A. Rulmont, R. Cloots, Morphological study of magnesium hydroxide nanoparticles precipitated in dilute aqueous solution, J. Cryst. Growth 249 (2003) 321–330, https://doi.org/10.1016/S0022-0248(02)02068-7.
[44] N.G. Özcan-Taşkin, G. Padron, A. Voelkel, Effect of particle type on the mechanisms of break up of nanoscale particle clusters, Chem. Eng. Res. Des. 87 (2009) 468–473, https://doi.org/10.1016/j.cherd.2008.12.012.
[45] A. Mersmann, Crystallization Technology Handbook, CRC Press, 2010.
[46] P.H. Karpiński, J. Bałdyga, Precipitation processes, Handb. Ind. Cryst, Cambridge University Press 2019, pp. 216–265, https://doi.org/10.1017/9781139026949.008.
[47] G.V. Lowry, R.J. Hill, S. Harper, A.F. Rawle, C.O. Hendren, F. Klaessig, U. Nobbmann, P. Sayre, J. Rumble, Guidance to improve the scientific value of zeta-potential measurements in nanoEHS, Environ. Sci. Nano 3 (2016) 953–965, https://doi.org/10.1039/c6en00136j.
[48] J.X. Lin, L. Wang, Adsorption of dyes using magnesium hydroxide-modified diatomite, Desalin. Water Treat. 8 (2009) 263–271, https://doi.org/10.5004/dwt.2009.786.
[49] G.A. Parks, The isoelectric points of solid oxides, solid hydroxides, and aqueous hydroxo complex systems, Chem. Rev. 65 (1965) 177–198, https://doi.org/10.1021/cr60234a002.
[50] V.A. Phillips, J.L. Kolbe, H. Opperhauser, Effect of pH on the growth of mg(OH)2 crystals in an aqueous environment at 60°C, J. Cryst. Growth 41 (1977) 228–234, https://doi.org/10.1016/0022-0248(77)90050-1.
[51] G.S. Smith, Human color vision and the unsaturated blue color of the daytime sky, Am. J. Phys. 73 (2005) 590–597, https://doi.org/10.1119/1.1858479.
[52] X. Pan, Y. Wang, Z. Chen, D. Pan, Y. Cheng, Z. Liu, Z. Lin, X. Guan, Investigation of antibacterial activity and related mechanism of a series of nano-Mg(OH)2, ACS Appl. Mater. Interfaces 5 (2013) 1137–1142, https://doi.org/10.1021/am302910q.